Neurobiology of Disease

Acute Focal Seizures Start As Local Synchronizations of Neuronal Ensembles

Michael Wenzel, Jordan P. Hamm, Darcy S. Peterka, and Rafael Yuste
Neurotechnology Center, Department of Biological Sciences, Columbia University, New York, New York 10027

Understanding seizure formation and spread remains a critical goal of epilepsy research. We used fast *in vivo* two-photon calcium imaging in male mouse neocortex to reconstruct, with single-cell resolution, the dynamics of acute (4-aminopyridine) focal cortical seizures as they originate within a spatially confined seizure initiation site (intrafocal region), and subsequently propagate into neighboring cortical areas (extrafocal region). We find that seizures originate as local neuronal ensembles within the initiation site. This abnormal hyperactivity engages increasingly larger areas in a saltatory fashion until it breaks into neighboring cortex, where it proceeds smoothly and is then detected electrophysiologically (LFP). Interestingly, PV inhibitory interneurons have spatially heterogeneous activity in intrafocal and extrafocal territories, ruling out a simple role of inhibition in seizure formation and spread. We propose a two-step model for the progression of focal seizures, where neuronal ensembles activate first, generating a microseizure, followed by widespread neural activation in a traveling wave through neighboring cortex during macroseizures.

Key words: **calcium imaging; epilepsy; interneurons; microseizures; seizures; two-photon**

Significance Statement

We have used calcium imaging in mouse sensory cortex *in vivo* to reconstruct the onset of focal seizures elicited by local injection of the chemoconvulsant 4-aminopyridine. We demonstrate at cellular resolution that acute focal seizures originate as increasingly synchronized local neuronal ensembles. Because of its spatial confinement, this process may at first be undetectable even by nearby LFP electrodes. Further, we establish spatial footprints of local neural subtype activity that correspond to consecutive steps of seizure microprogression. Such footprints could facilitate determining the recording location (e.g., inside/outside an epileptogenic focus) in high-resolution studies, even in the absence of a priori knowledge about where exactly a seizure started.

Introduction

Understanding the properties of seizure-producing cortical circuits ("epileptic networks") may enable more efficient seizure control. Although cortical circuits are complex in terms of cell types and connectivity, little is known about the neural subpopulation dynamics within epileptic networks *in vivo* (Muldoon et al., 2015; Neumann et al., 2017), especially in relation to the seizure initiation site and surrounding brain tissue. However, how exactly seizures progress from microscale to macroscale in the intact brain may hold critical new clues on how to stop their expansion.

Seizures often emerge at locally confined epileptic foci, from where they can secondarily spread across the brain. But, due to technical limitations, our knowledge about the precise dynamics of local brain networks in and outside such foci is still scarce. Recent technology advances have enabled more fine-scaled studies of these dynamics leading for example to the identification of "microseizures" (Goldensohn, 1975; Schevon et al., 2008; Worrell et al., 2008; Stead et al., 2010). Microseizures display field-electrographic features similar to seizures detected in the EEG, yet are clinically silent and territorially too confined to be detectable by conventional macroelectrodes (Stead et al., 2010). Thus, a deeper understanding of seizure emergence and spread at a neural circuit level requires techniques with high spatiotemporal resolution. Although multielectrode arrays have pushed our understanding of fine-scale epileptic network dynamics, most common configurations (96 electrodes, 4 × 4 mm) do not allow measurements of complete neural circuits. In fact, such arrays usually record from several dozen (at best up to ~180) neurons from patches of cortex or hippocampus (Truccolo et al., 2011;

Received Dec. 17, 2018; revised July 27, 2019; accepted Aug. 9, 2019.

Author contributions: M.W. and R.Y. designed research; M.W. performed research; M.W., J.P.H., and D.S.P. analyzed data; M.W., J.P.H., D.S.P., and R.Y. edited the paper; M.W. wrote the paper.

This work was supported by the Deutsche Forschungsgemeinschaft (DFG, Grant WE 5517/1-1), NEI (DP1EY024503, R01EY011787), NIMH (R01MH101218, R01MH100561, R01MH115900), and DARPA SIMPLEX N66001-15-C-4032. This material is based upon work supported by, or in part by, the U.S. Army Research Laboratory and the U.S. Army Research Office under contract number W911NF-12-1-0594 (MURI). We thank Yeonsook Shin, Alexa Semonche, Reka Recinos, Mari Bando, and Azadeh Hamzei for viral injections and members of the Yuste laboratory for useful comments.

M. Wenzel's present address: Department of Epileptology, University of Bonn, 53127 Bonn, Germany.

Correspondence should be addressed to Michael Wenzel at michaelwenzel2946@gmail.com.

https://doi.org/10.1523/JNEUROSCI.3176-18.2019

Neumann et al., 2017), which, however, contain hundreds of thousands of neurons. Due to this, and the usually spatially poor identification of seizure initiation sites before electrode implantation in patients or animals, it has remained unclear how seizures emerge and transition from focal epileptic discharges to secondarily generalized seizures. As an alternative to electrophysiology, calcium imaging can monitor action potential activity with single cell resolution (Yuste and Katz, 1991; Smetters et al., 1999), so it seems as an ideal method to map seizures and epileptic spread, cell by cell, at the anatomical microscale (Badea et al., 2001). However, calcium imaging studies of epileptic activity have traditionally suffered from a temporal resolution too low to investigate sizable population dynamics during seizures (Badea et al., 2001; Tashiro et al., 2002; Trevelyan et al., 2007; Cammarota et al., 2013; Feldt Muldoon et al., 2013; Neubauer et al., 2014; Lillis et al., 2015; Muldoon et al., 2015). To improve the temporal resolution of calcium imaging, we recently introduced a fast (30 Hz) resonant scanning method to study cortical seizure propagation *in vivo* (Wenzel et al., 2017). In that initial study, general local network recruitment patterns to spreading acute seizures were investigated at a distance ("propagation area") to a spatially confined seizure initiation site. We found that in the propagation area, seizure spread occurs in a continuous fashion, through stereotypical circuits, and that this spread is elastic in time and regulated by the activity of GABAergic interneurons.

Here, we turn our attention to the initiation site ('intrafocal') of cortical seizures, and compare the findings to recruitment patterns within the propagation area ("surround cortex" or "extrafocal"). To compare seizure progression at the anatomical microscale ('microprogression') in both these compartments, we use fast (30 Hz) two-photon calcium imaging of GCaMP6-labeled neuronal populations of mouse somatosensory cortex and LFP recordings in the 4-aminopyridine (4-AP) mouse model of acute focal onset seizures *in vivo*. The approach combines high temporal and single cell resolution to unveil the local population activity underlying seizures with unequivocal anatomical precision. With a precisely defined focal seizure onset zone by local cortical 4-AP injection (Nagappan et al., 2018, see also methods), we image cortical circuits within the seizure initiation site as well as the propagation area that is invaded only during seizures detected by nearby microelectrodes. Further, we perform subpopulation calcium imaging of td-Tomato labeled PV interneurons within those territories during seizure emergence and spread, and find spatially heterogeneous PV recruitment. Our data represent a complete reconstruction of seizure progression from their microepileptic origins, and have potential implications for the early detection of pending seizures through the establishment of local footprints of neuronal subpopulation activity patterns throughout seizure evolution.

Materials and Methods

Experiments. All experiments were performed with care and in compliance with the Columbia University institutional animal care guidelines. Experiments were performed on either male C57BL/6 wild-type mice (Jackson Laboratories; RRID:IMSR_JAX:000064) or male PV-Cre::LSL-tdTomato mice (Jackson Laboratories; PV-Cre mice: RRID:IMSR_JAX:017320; LSL-tdTomato mice: RRID:IMSR_JAX:007908) at a postnatal age of 1–3 months. Animals were never used for previous or subsequent experiments. Food and water was provided *ad libitum*. Mice were housed at a 12 h light/dark cycle. Calcium transients and LFP signals from three GCaMP6s monolabeled animals, in which general, extrafocal seizure progression was compared with intrafocal dynamics in this paper, were also used in our previous study that exclusively investigated seizure progression in extrafocal territories ("propagation area") (Wenzel et al., 2017). All intrafocal imaging experiments and double-labeled animals for subpopulation imaging were exclusively used for the study presented here.

Specification of terms related to epileptic activity used in this study. This paper contains numerous different terms referring to epileptic activity. We would like to specify here how particular terms were used:

"Ictal activity": the Latin term "ictus" refers to a sudden attack, and is used for epileptic seizures in clinical epileptology. We used the adjective "ictal" exclusively in the context of seizure activity. The term 'interictal' refers to epileptic activity in between seizures. We made use of the term "pre-ictal" (as part of the interictal period) with reference to the time period immediately preceding the electrographic seizure onset in the LFP.

"Epileptic activity": The term "epilepsy" comprises both interictal and ictal activity. The adjective "epileptic" was used here as an umbrella term for both pre-ictal and ictal neural activity. For escalatory aberrant intrafocal calcium activity patterns during pending LFP seizure onset at the nearby microelectrode, we used the term 'epileptic' activity, as in our dual (calcium imaging, LFP) recordings the delineation between pre-ictal and ictal activity became less clear. We used the term "micro-epileptic" to emphasize the spatial dimension of our calcium imaging at the anatomical scale of dozens to hundreds of micrometers.

"Microseizures": Microseizures display field-electrographic features similar to seizures detected in the EEG, yet are clinically silent and territorially too confined to be detectable by conventional macroelectrodes, or even nearby microelectrodes (e.g., at 1 mm distance; Stead et al., 2010). Macroseizures represent seizures that can be detected by microelectrodes and macroelectrodes across wider portions of the brain.

Virus injections and surgical procedures. Before actual experiments, animals were injected with AAV1-Syn-GCaMP6s-WPRE-SV40 (purchased from the University of Pennsylvania Vector Core). Mice were anesthetized with isoflurane (initial dose 2–3% partial pressure in air, then reduction to 1–1.5%). A small cranial aperture was established above left somatosensory cortex (coordinates from bregma: x 2.5 mm, y −0.24 mm, z −0.2 mm) using a dental drill. A glass capillary pulled to a sharp micropipette was stereotactically lowered into cortical layer 2/3. An 800 nl solution of 1:1 diluted AAV1-Syn-GCaMP6s (Chen et al., 2013) was slowly injected over 5 min at a depth of 200 μm from the pial surface using a microinjector (World Precision Instruments). Four to 5 weeks after virus injection, on the day of the experiment, mice were anesthetized with isoflurane (initial dose 2–3% partial pressure in air, then reduction to 1.0%). A small flap of skin above the skull was removed and a titanium head plate with a central foramen (7 × 7 mm) was attached to the skull with dental cement above the left hemisphere (Fig. 1*A*). Then, a small craniotomy similar to previous descriptions (Miller et al., 2014) was carried out. Specifically, posterior to the virus injection site, the skull was circularly thinned using a dental drill until a small piece (~2 mm in diameter) of skull could be removed effortlessly with fine forceps.

Two-photon calcium imaging. Activity of cortical neurons was recorded by imaging changes of fluorescence with a two-photon microscope (Bruker Instruments) and a Ti:Sapphire laser (Chameleon Ultra II; Coherent) at 940 nm through a 25× objective (water-immersion, numerical aperture 1.05, Olympus). Resonant galvanometer scanning and image acquisition (frame rate 30 fps, 512 × 512 pixels, 100–170 μm beneath the pial surface) were controlled by Prairie View Imaging software. Multiple datasets were acquired consecutively over the course of an experiment (90,000–150,000 frames in total, with several momentary breaks interspersed for reasons of practicality). During the entire experiment, the head-restrained animals were kept under light isoflurane anesthesia (0.8–1% partial pressure in air) via a nose piece while body temperature was maintained with a warming pad (37.5°C).

Ictal model and electrophysiology. The local 4-AP model of acute cortical seizures was used in this study, as it allowed the precise localization of the seizure initiation site and propagation area. We primarily defined the seizure initiation site as the location of 4-AP injection (15 mM, 500 nl, layer 4 or 5, total amount delivered = 7.5nmol), and the propagation area as an area at 1.5–2 mm distance, which is primarily unaffected by 4-AP (Nagappan et al., 2018), but invaded during secondary lateral seizure spread as described previously (Wenzel et al., 2017). In the context

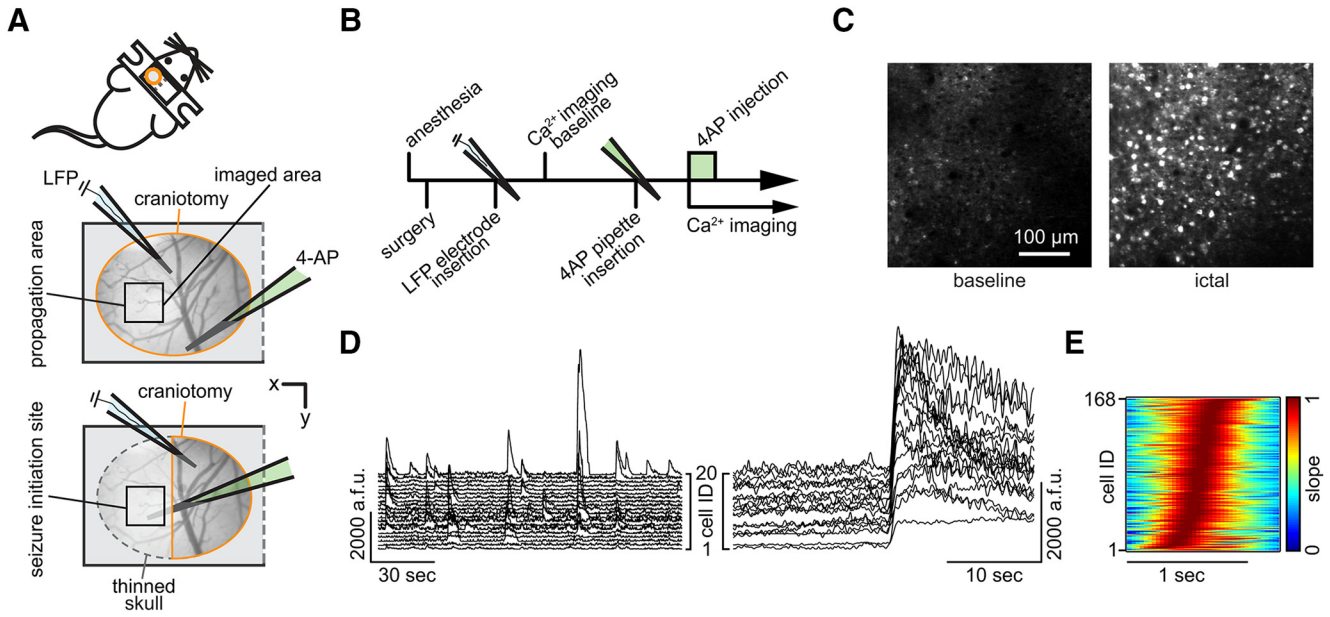

Figure 1. Imaging in the seizure initiation site and propagation area. ***A***, Experimental setup. Two surgical approaches over left somatosensory cortex; craniotomy encircled in orange, thinned skull in dotted gray, black squares indicate imaged FOV; each experiment (exp.) involved the insertion of two glass micropipettes, one (blue) containing a silver chloride silver for LFP recording, the other (green) containing 4-AP (15 mM, injection vol. 500 nl, total amount delivered = 7.5nmol). ***B***, Experimental workflow. ***C***, Propagation area, representative 3 s average (avg) fluorescence images of neural activity (GCaMP6s) during baseline and ictal break-in. ***D***, Calcium (Ca^{2+}) transients of 20 representative cells during baseline conditions (left) and during ictal invasion of the propagation area (right). a.f.u., Arbitrary fluorescent units. ***E***, Propagation area, representative example of the arriving ictal wavefront. Normalized first derivative of each registered neuron's fluorescent trace during electrographic seizure onset is shown. Cell recruitment to ictal activity ordered in time by maximum slope. Note the s-curved shape of cell recruitment highlighting sufficient temporal imaging resolution for individual cellular recruitment.

of the 4-AP model used here, it is further noteworthy that seizure occurrence in chronic animal models of epilepsy is usually low (Arida et al., 1999; Ewell et al., 2015; Muldoon et al., 2015). It would require either multiple fortunate or prohibitively long imaging sessions of infrequently occurring spontaneous seizures to capture a sufficient number of seizures, along with reasons concerned with potential tissue photo-damage, fluophore bleaching and hardware limitations. For LFP recordings, a sharp glass micropipette (2–5 MΩ) filled with saline and containing a silver chloride wire was carefully advanced into the cortex (30° angle) under visual control to a depth of ~100 μm beneath the pial surface. The pipette tip was positioned close by the imaged area (Fig. 1*A*). A reference electrode was positioned over the contralateral prefrontal cortex. In the context of this paper, the term "electrographic" specifically refers to LFP signals recorded by sharp glass micro-electrodes as described above. LFP signals were amplified using a Multiclamp 700B amplifier (Molecular Devices), low-pass filtered (300 Hz, Multiclamp 700B commander software, Molecular Devices), digitized at 1 kHz (Bruker Instruments) and recorded using Prairie View Voltage Recording Software alongside with calcium imaging. For induction of seizures, another sharp glass micropipette containing 4-AP (15 mM, 0.5 μl) was slowly lowered (30° angle) into the cortex to a depth of 420–480 μm. The pipette tip was positioned at a distance of ~1.5–2 mm caudally to the imaged area. Correct positioning of the pipette tip was ensured by a diagonal dry-run within saline above the cortex preceding actual insertion. 4-AP was injected over the course of 10–15 min by use of a Micro4 Micro Syringe Pump Controller (World Precision Instruments). Electrographic seizure onset time points were determined mathematically by mean and SD of LFP recordings. The first time point exceeding > 5 SD from the interictal LFP mean power was defined as the electrographic seizure onset and confirmed by visual inspection. We did not determine seizure onsets based on calcium imaging, but analyzed neural calcium transients with reference to the electrographic seizure onset in the LFP, as field electrophysiology represents the most widely accepted method to detect the temporal onset of seizures.

Focality of the local cortical 4-AP model. It is difficult to prove that no 4-AP reached the imaged field of view in the propagation area ("extrafocal") throughout our experiments. However, a number of points support that this area was indeed not primarily affected by 4-AP in our setting. We locally injected small amounts of 4-AP (7.3 nmol) into deep layers, and imaged in layer 2/3 at a distance of 1.5–2 mm. We only found enhanced extrafocal pyramidal activity during secondary seizure spread. By contrast, we immediately observed increased neural firing upon 4-AP injection in the initiation site. One could argue that our observed network compartmentalization might be driven by a 4-AP concentration gradient, for example, preferentially activating extrafocal PVs leading to surround network suppression. However, Nagappan et al. (2018) recently showed in the identical seizure model that fluorescently labeled 4-AP hardly diffuses beyond 1 mm from the injection site over 2 h. At the same time, Liou et al. (2018) found enhanced PV firing even at an ~4 mm distance to ongoing focal cortical seizures. Finally, we recently showed slow seizure propagation in the disinhibitory local picrotoxin (Ptx) model (Wenzel et al., 2017), where, if the propagation area had primarily experienced Ptx, seizure progression would have been rapid, and interictal LFP spikes would have recruited local pyramidal neurons. However, such recruitment only occurred upon a second Ptx injection in the initiation site (picospritzer, 10 psi, 10 min).

Image analysis. Cell regions of interest (ROIs) were identified in a semiautomated fashion by using custom written software in MATLAB (Caltracer 3 β, available on the Yuste laboratory website at https://blogs.cuit.columbia.edu/rmy5/) followed by manual confirmation. Because of pronounced and synchronous fluorescence changes of surround neuropil during epileptic conditions, halo subtraction procedures could lead to distortions of calcium transients of individual cells. Therefore, we applied ROI shrinkage (ROI soma outline minus 1.5 pixels radially), which has been successfully used to minimize bleed-in of surround neuropil fluorescence (Hofer et al., 2011). Cells with low signal-to-noise ratio or no apparent calcium transients were excluded from further analysis. Individual cells that were lost over the course of the experiment due to at times discrete axial movement of the imaged focal plane during local 4-AP injection were also excluded from further analysis. Individual cell fluorescence was calculated as the average across all pixels within the ROI.

Cell recruitment analyses. To determine the recruitment time-point of individual cells to ictal activity, we used the first discrete derivative (slope) of the individual fluorescent traces assuming that the sharpest

change in fluorescence correlates best with maximal recruitment to seizure activity (Trevelyan et al., 2006; Wenzel et al., 2017). Population recruitment durations were calculated as the time from the first to the last recruited registered cell, excluding the 5% most deviant cells to reduce outlier-induced duration distortions. Specific time lags of PV neural recruitment compared with local network recruitment to seizure activity were calculated as previously described (Wenzel et al., 2017): First, we derived the median frame Y_{50} wherein the cumulative number of recruited cells first equaled or exceeded 50% of all registered neurons. Then, relative to this Y_{50}, each PV was assigned a temporal recruitment lag by subtracting Y_{50} from its individual recruitment frame X_N ($X_n - Y_{50}$, a negative result would indicate an early recruitment of the respective PV ahead of the median population recruitment for a given seizure event).

Spatiotemporal clustering. To identify spatio-temporo-progressive network activity motifs during seizure microprogression, we ordered cell recruitment points in time (from early to late recruitment) during each individual ictal event of an experiment and divided each dataset into four groups (1–25%, 26–50%, 51–75%, 76–100%), as previously described (Wenzel et al., 2017). Then, the mean distance of cell coordinates (x, y within imaged area) of individual quartiles were calculated to either the mean coordinate of the respective quartile, or the mean coordinate of all recorded cells, for each seizure. These distances were compared with each other. If cells' recruitment time points are similar and cells cluster spatially, their distance to the mean coordinate of their respective quartile should be significantly shorter than the mean distance to the mean coordinate of all cells that are distributed over the entire field of view (Fig. 2*G*).

PCA and state space. We sought to parsimoniously describe multicellular network dynamics in a lower rank subspace amenable to visual display and linear comparisons. Using in-house written MATLAB routines and standard functions, we calculated a principle components analysis (PCA) on cells × time points activity matrices (i.e., cells were variables) separately for baseline (preinjection) activity, the 40 s period before LFP seizure onset, and 3 s after seizure onset. We examined scree plots to quantify the proportion of variance accounted for by each component (Cattell, 1966), comparing root eigenvalues between conditions to assess an indication of dataset dimensionality. In all three cases, the scree-test suggested 2 components (although the variance of network activity at baseline was ostensibly spread across more components than preictal and postictal periods). For plotting and visualizing the nature of the multicellular propagation patterns (i.e., similarities, differences, and the periodic structure of their build up; Fig. 3*A*,*B*), we performed a VARIMAX rotation (Kaiser, 1958) to limit PCA solutions to two components (based on scree test; a 2D solution is also conveniently easier to visualize). This approach simplifies the PCA solution to include fewer components (in this case, two, which remain orthogonal) by rotating factor weights in a manner that maximizes the summed variances of the squared loadings.

Statistics. All data were analyzed using custom written code in MATLAB (The MathWorks). Error bars on bar plots and shaded areas in graph plots indicate SEM. To determine statistical significance for analyses regarding cell recruitment, Mann–Whitney tests were applied unless stated otherwise. For statistical analysis of spatio-temporal clustering, we used bivariate ANOVA analysis of mean distance differences (df = 3). High activity subtype comparison (Figs. 4, 5) was determined by χ^2 test (1 degree of freedom [df]).

Additional resources. MOCO (ImageJ plugin for motion correction) is available online on the Yuste laboratory website.

Results

This study used optical and electrical techniques to record focal seizure emergence and spread, and contains the terms "electrographic," "microseizure," "macroseizure," "micro-epileptic," "epileptic," "pre-ictal," and "ictal." To avoid confusion as to how these terms were used in the context of this work, respective definitions are provided in the methods section. The data shown here represent a total of 13 experiments. Six animals were studied for general intrafocal or extrafocal recruitment to epileptic activity (898 distinctly registered neurons), and seven animals were used for subpopulation imaging (1059 distinctly registered neurons, of which 79 were PVs). We used an *in vivo* mouse model of acute cortical seizures applying local injection of 4-AP (15 mM, 500 nl, layer 4 or 5, total amount delivered = 7.5 nmol) in lightly anesthetized mice. We performed experiments under light anesthesia to reduce the animal burden of a series of prolonged tonic-clonic seizures and given that seizures in humans do not only happen during wakefulness, but are also encountered in seizure-susceptible individuals even during deeper anesthesia on the intensive care unit or in the operation room (Howe et al., 2016; Ulkatan et al., 2017). Further, we and others have previously provided some evidence that despite differences such as seizure threshold or propagation speed, general neural recruitment patterns during cortical seizure progression share fundamental characteristics across anesthesia and wakefulness (Uva et al., 2013; Wenzel et al., 2017). The 4-AP model was chosen for several reasons (see the Materials and Methods). First, local injection of small amounts of 4-AP establishes a territorially well defined acute epileptic focus surrounded by primarily unperturbed cortex that is invaded during electrographic seizures (Wenzel et al., 2017; Nagappan et al., 2018). Although not recapitulating chronic epilepsy, the acute situation established by focal 4-AP resembles real world medical conditions such as intracerebral bleeding, local brain trauma or ischemic stroke, in which acute seizures often occur shortly after the injury (Beleza, 2012). The model also shares some similarities with chronic conditions such as epilepsy with focal onset seizures, where spatially confined epileptic discharges secondarily spread into otherwise functionally intact brain tissue (Milton et al., 2007). Moreover, unlike disinhibitory chemoconvulsants such as picrotoxin or bicuculline, 4-AP leaves inhibitory circuits intact, and elicits electrographic and behavioral phenomena that are similar to seizures in chronic epilepsy (Szente and Pongrácz, 1979; Avoli et al., 2002). Instead of addressing a specific disease pathway but rather considering epileptic seizures as a phenomenon shared by many neurological disorders and even the healthy brain, our model focused on understanding the phenomena of epileptic states (Jirsa et al., 2014).

Two-photon calcium imaging within the local seizure initiation site *in vivo*

Two experimental setups were used including either a craniotomy for imaging within the propagation area or a craniotomy combined with adjacently thinned skull for intrafocal imaging (Fig. 1*A*). In both setups, imaging was performed in layers 2/3 (L2/3, ~150 μm beneath the cortical surface) of mouse primary somatosensory cortex. The experimental workflow is depicted in Figure 1*B*. For LFP measurements, which served as the electrographic indicator of seizures within the investigated cortical territory, a sharp glass microelectrode was carefully lowered into the cortex close by the imaged area. Whenever the term "electrographic" is used throughout this paper, it refers to the recorded LFP signal. For induction of seizures, a second glass micropipette containing 4-AP (total amount delivered = 7.5 nmol) was slowly advanced to a cortical depth of ~480 μm. The tip of the 4-AP pipette was either positioned at a distance of ~1.5–2 mm caudally to the field of view (propagation area) or directly underneath the imaged area (initiation site). During baseline conditions, local populations in L2/3 displayed ongoing sparse and distributed calcium activity (Fig. 1*C*,*D*, left; Miller et al., 2014), contrasted by sustained firing of large numbers of neurons in the field of view

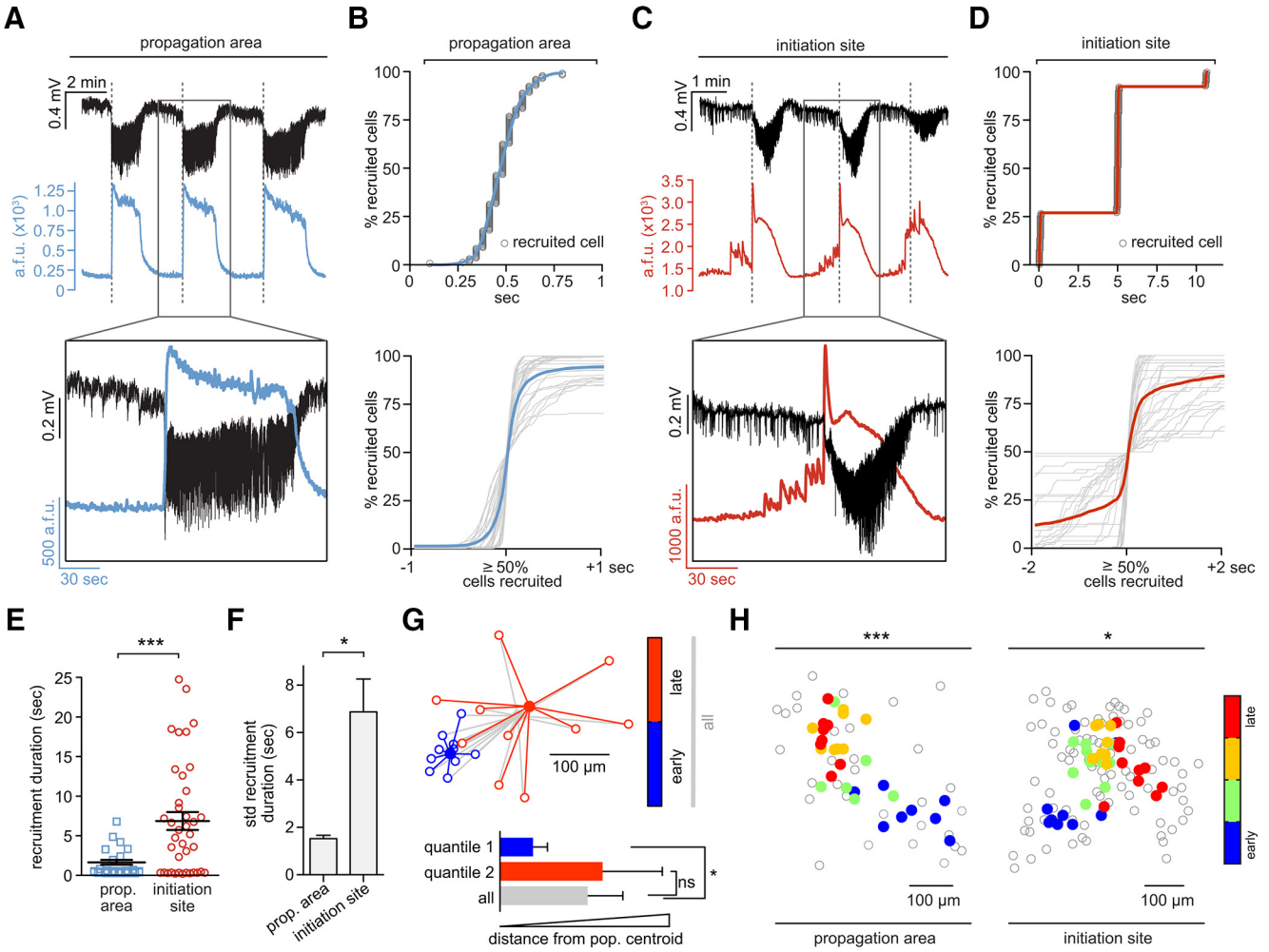

Figure 2. Differential intrafocal and extrafocal neuronal recruitment during seizure micro-progression. ***A***, Propagation area: LFP signal (black), and corresponding population avg. Ca^{2+} transient (blue) of three consecutive seizures, detailed depiction of second event (inset, see also Movie 1). Note how electrographic seizure onsets (dotted lines) correspond to the sudden rise of the population Ca^{2+} signal. a.f.u., Arbitrary fluorescent units (***B***) Propagation area. Top, Representative example of smooth, s-shaped cell recruitment during ictal break-in. Bottom, Superposition of neural recruitment curves across all analyzed ictal break-ins (gray) centered around the 50% recruitment frame; blue graph represents mean [$n = 3$ exp., total number of seizures = 31 (10.3 ± 1.5275 SEM)], cell number in percentage for comparability across exp.). ***C***, Initiation site: LFP recording (black) and corresponding avg. population Ca^{2+} transient (red) of three consecutive seizures, detailed depiction of second event (inset, see also Movie 2). Note the temporal mismatch of electrographic seizure onsets and intrafocal population Ca^{2+} events. Large pre-ictal population bursts are visible before the electrographic seizure onset (dotted line). ***D***, Top, Representative example of stepwise cell recruitment during intrafocal micro-epileptic progression. Bottom, Superposition of all analyzed intrafocal epileptic recruitment (gray) centered around the 50% cell recruitment frame; red graph represents mean (3 exp., total number of seizures = 39 [13 ± 1.55 SEM]). ***E***, Comparison of extrafocal vs intrafocal cell recruitment durations ($n = 31$ vs 39 durations; mean 1.83 ± 0.3 s vs 6.82 ± 1.1 s, Mann–Whitney test $p < 0.001$). Determination of recruitment durations was done by calculating the time period from the first to last recruited registered cell, excluding the 5% most deviant cells. ***F***, Comparison of extrafocal versus intrafocal recruitment duration variability (mean SD ± SEM, Mann–Whitney test $p < 0.05$). ***G***, Schematic depiction of bivariate cluster analysis. For practical visualization, only 2 quantiles (blue = 50% earliest, red = 50% latest recruited cells) are displayed for an individual seizure (actual exp. contained 4 quantiles). Each quantile contains 10 cells. Each outlined circle corresponds to the spatial coordinate of an individual cell, each filled circle to the respective quantile centroid (blue, first quantile; red, second quantile; gray, all; centroid, mean spatial coordinate). Note: quantiles were calculated based only on temporal onset, regardless of space. Bottom panel: Arbitrary mean distance + SD for each quantile for the single seizure shown on top (actual analysis contained all seizures of an individual experiment). Cells belonging to the early 50th percentile (blue) cluster spatially, cells belonging to the late 50 percentile (red) do not. ***H***, Left, Spatial analysis of propagation area: Spatiotemporal quartile clustering (quartiles calculated as mean coordinate of 1–25% earliest cells, 25–50%, 50–75% and 75–100%, see Materials and Methods) across 8 consecutive seizures (bivariate ANOVA $p < 0.001$, all extrafocal exp. $p < 0.05$). Right, Spatial analysis of initiation site: Spatiotemporal quartile clustering (each quartile coordinate = spatial mean of 25% recruited cells) clustering across 10 consecutive seizures (bivariate ANOVA $p = 0.0145$, all intrafocal exp. $p < 0.05$). Depiction of statistical significance for Figure 2: *$p < 0.05$; ***$p < 0.001$.

during electrographic seizures post 4-AP injection (Fig. 1*C*,*D*, right). Within the propagation area, seizure invasion happened in a wave of burst neuronal firing advancing slowly (Wong and Prince, 1990; Trevelyan et al., 2007; Wenzel et al., 2017) across the field of view (see Movie 1). The temporal imaging resolution of 30 Hz was sufficient to capture individual cell recruitment to epileptic activity (Fig. 1*E*). We focused on early seizure cell recruitment and recruitment immediately preceding electrographic seizures (time window 40 s before and 10 s into individual electrographic seizures), since this window represents a critical time for potential therapeutic interventions. To systematically investigate general temporal characteristics of microprogression of epileptic activity, we analyzed the activity of all neurons in the field of view that showed visible calcium transients during epileptic activity and whose somata could be followed across the entire experiment. Individual cell recruitment time-points were derived by calculating the first discrete derivative (slope) of the fluorescent traces assuming that the steepest rise in fluorescence correlates best with maximal recruitment to epileptic activity (Badea et al., 2001; Trevelyan et al., 2006; Wenzel et al., 2017).

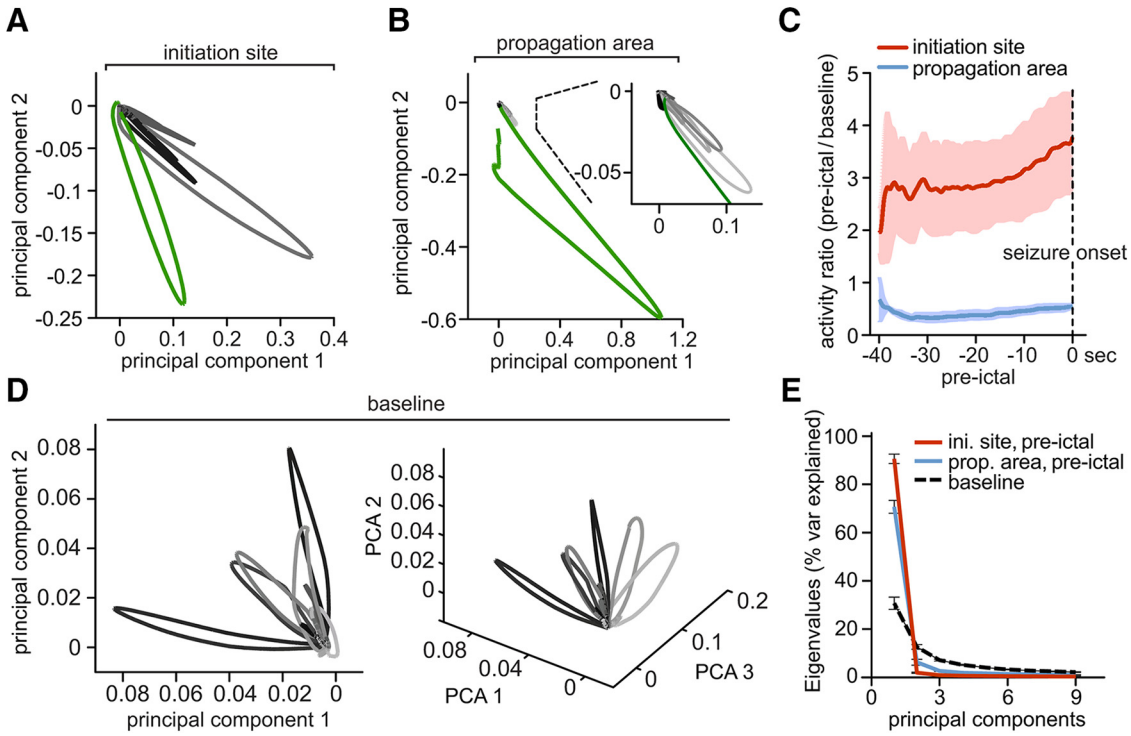

Figure 3. Pre-ictal local networks compartmentalize and decline into lower dimensional attractors. ***A***, Representative network state spaces [40 s pre-ictal state changes in grayscale (black = earliest change), electrographic seizure onset in green] within the seizure initiation site and (***B***) the propagation area, with a magnified inset. Every data point along a given trajectory corresponds to the imaged population activity at a single time point (for details on PCA component space visualization please see methods). Note two important local network features visualized in ***A*** and ***B*** at once: pre-ictal network activity dimensionality is reduced in both initiation site and propagation area; however, intrafaocal network activity shows large trajectories before electrographic seizure onset while extrafocal activity appears to be suppressed. ***C***, Cumulative frame-population-averaged positive change of fluorescence, normalized to baseline (set to 1), as indicator of general relative network activity changes over time (GCaMP6s, 3 extrafocal/3 intrafocal exp., 29/39 pre-ictal periods). Pre-ictal intrafocal vs extrafocal network activity was compared by a running *t* test ($p < 0.001$ from −34 to 0 s). ***D***, Representative network state space (2D on the left, same space in 3D on the right) with individual network events (in gray scale) over a 40 s period during baseline. In contrast to the pre-ictal condition displayed in ***A*** and ***B***, activity trajectories reach out into all plotted dimensions. ***E***, Scree plot of principial components of baseline network activity versus pre-ictal intrafocal vs extrafocal activity. Note the reduced number of principal components in both pre-ictal conditions. Displayed components accounted for >90% of the variance, respectively.

Seizure initiation and propagation areas display differential spatiotemporal dynamics

In the propagation area, electrographic seizures and calcium transients corresponded well and neurons in the propagation area were recruited in a continuous fashion (Fig. 2*A* and *B*, top) (Wenzel et al., 2017). Before ictal invasion during electrographic seizures, little to no calcium activity was visible in the propagation area. To analyze this, we superimposed the calcium activity for all experiments in the propagation area around the frame where the proportion of neurons recruited to ictal activity reached 50%. The superimposed graphs lined up consistently, describing a continuous s-shaped curve (Fig. 2*B*, bottom, $n = 3$ experiments; GCaMP6s; total number of seizures = 31; average number of seizures = 10.3 ± 1.5275; total number of analyzed cells = 576; average number of analyzed cells = 192 ± 58.9237), as previously described (Neumann et al., 2017; Wenzel et al., 2017).

The seizure initiation site, however, displayed strikingly different activity patterns (Fig. 2*C*) (Warren et al., 2010). Unlike the propagation area, we observed here locally restricted, pronounced bursts of activity, sometimes long before electrographic seizure onset (Fig. 2*C*, Movie 2). These events reflected sustained, abnormal local population activity that evolved in space and time, which are typical EEG hallmarks of seizure activity. Further, intrafocal epileptic buildup consistently occurred before electrographic seizure onset. Moreover, neurons within the seizure initiation site were recruited in a stepwise pattern (Fig. 2*D*, top). When we superimposed all imaged intrafocal neuronal activity around the 50% recruitment frame, a discontinuous pattern emerged from highly variable individual recruitment graphs (Fig. 2*D*, bottom, $n = 3$ experiments, GCaMP6s, total number of seizures = 39, average number of seizures 13 ± 1.55, total number of analyzed cells = 272, average number of analyzed cells = 91 ± 23 cells). Neuronal recruitment was temporally stretched, up to dozens of seconds ahead of the LFP seizure onset (Fig. 2*E*), and significantly surpassed the already considerable variability of neuronal activation across seizures within the surround cortex (Wenzel et al., 2017) (Fig. 2*F*).

We compared the spatiotemporal maps of successive seizures between the propagation area and the seizure initiation site and found that, despite the different types of seizure progression, a conserved spatial pattern of relative cell recruitment was evident in both compartments across seizures (Fig. 2*G*,*H*) (Trevelyan et al., 2006; Truccolo et al., 2014; Neumann et al., 2017; Wenzel et al., 2017). To quantify and compare these observed spatiotemporal patterns, we used a 2-dimensional ANOVA (Wenzel et al., 2017), categorizing cells into temporal quartiles and comparing the variance of the distance of each cell with the quartile spatial mean and with the variance of the distance to the spatial mean of all cells (Fig. 2*G*). The analysis yielded significant differences between distributions, with bivariate F-values for all experiments in the propagation area ($F = 12.67, 11.64, 41.22$; all $p < 0.001$) and in the seizure initiation site ($F = 22.15, 4.02, 3.43$; $p = 1.4 \times 10–9, 0.0145, 0.024$) (Fig. 2*H*).

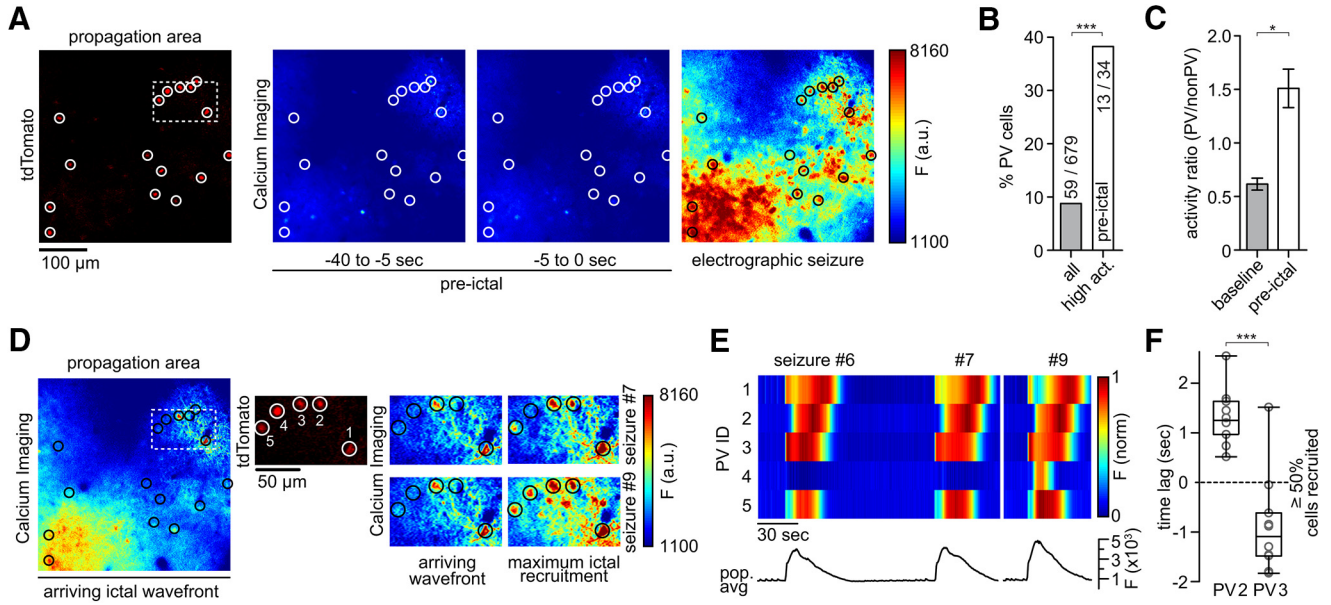

Figure 4. Ictal recruitment of PV interneurons in the propagation area. ***A***, Left to right, tdTomato-positive parvalbumin-containing interneurons (PVs, encircled), imaged at 990 nm; Ca^{2+} imaging (at 940 nm): fluorescence avg. images during pre-ictal period and ictal activity. ***B***, PV percentage among highest active neurons during pre-ictal period ($n = 4$ experiments, total number of pre-ictal periods = 30 [7.5 ± 1.85 SEM], all imaged non-PVs = 620, PVs = 59, top 5% activity cells = 34) compared with general subtype distribution (χ^2 test $p(\chi^2 > 39.381) < 0.001$). ***C***, Activity ratio of PV versus non-PV subpopulations during baseline and the 40 s period before seizure onset. Activity ratios were obtained by dividing frame-subpopulation-averaged positive change of Ca^{2+} fluorescence. During baseline (left), PVs continually display lower values than non-PVs. During the pre-ictal period (right), this relationship is inverted ($n = 4$ exp., GCaMP6s, 30 pre-ictal periods, Mann–Whitney test $p = 0.0286$). ***D***, Same exp. as in A, during ictal break-in (left); middle and right side: insert shown in ***A*** and ***D*** (dotted box). Displayed are 5 immediately neighboring PVs and their Ca^{2+} transients during ictal break-in and sustained ictal activity across 2 successive seizures (upper and lower panel, see also Movies 4 and 5). Note the diverse PV recruitment to ictal activity with PV #1 and #3 bursting ahead of the arriving ictal wavefront, PV #2 and #5 showing delayed recruitment (intraictal section), and one nonparticipant PV (#4) during the first seizure. The latter cell is clearly recruited to a successive ictal event. ***E***, Bottom, Population avg. Ca^{2+} fluorescence signal of all 124 registered cells from exp. shown in A and D across 3 seizures (#6, 7,and 9). Top, Max-normalized Ca^{2+} fluorescence for the 5 PVs highlighted in D, shown across 3 seizures. Note the differential recruitment on the order of seconds of even immediately neighboring PVs. PV #4 does only show a clear Ca^{2+} signal in the last seizure displayed (***F***) Differential relative recruitment (Time lag with respect to the 50% recruitment frame) of immediately neighboring PV #2 and #3 (intercell distance <50 µm, both cells are located far from the arriving ictal wavefront within the imaged area) across all seizures of the exp. (10 seizures, Mann–Whitney test $p < 0.001$). Boxes represent 25th to 75th percentile of cellular recruitment, bands inside boxes display median cell recruitment time points, circles represent cell recruitment time lag for individual seizures. Depiction of statistical significance for Figure 4: $*p < 0.05$; $***p < 0.001$.

In sum, we found a saltatory expansion of abnormal neural population hyperactivity within the seizure initiation site followed by a continuous invasion of surround cortex. Within the seizure initiation site, spatially restricted bursts of population activity occur up to dozens of seconds before LFP seizure onset, with highly variable, stretched courses of neural recruitment in absolute time. In stark contrast, in the surround cortex, preseizure activity is low and neural recruitment occurs only during electrographic seizures. Despite differential types of microprogression of epileptic activity, the relative spatiotemporal activity patterns of local networks show consistency across seizures in both intrafocal and extrafocal compartments.

Preseizure subnetwork compartmentalization and critical state transitions

The differential intrafocal and extrafocal subnetwork activity before LFP seizure onset prompted us to further investigate the mechanisms underlying these population dynamics. To this end, we analyzed the neuronal correlation in the calcium imaging data by applying principal component analysis (PCA; Materials and Methods, Fig. 3*A–C*) to 40 s preseizure periods. PCA weights were calculated within an experiment across all seizures and applied in time to simplify the "state-space" of multidimensional population activity occurring before and during LFP seizure onset (Fig. 3*A*,*B*). Compared with extrafocal network activity (Fig. 3*B*, grayscale, electrographic seizure onset in green), which was sparse (Bower and Buckmaster, 2008; Schevon et al., 2012) and correspondingly did not show clear excursions in state space before LFP seizure onset, intrafocal population dynamics showed large state space trajectories (Fig. 3*A*, grayscale) corresponding to sustained abnormal hyperactivity evolving in time and space toward the electrographic seizure onset (green). Accordingly, during the 40 s before electrographic seizure onset, intrafocal average population activity was persistently higher than during baseline and escalated noticeably toward seizure onset (Fig. 3*C*, red trace). On the contrary, at the same time, extrafocal population activity in surround cortex was in fact steadily lower than during baseline conditions (Fig. 3*C*, blue trace).

However, compared with baseline conditions, where a great diversity of network states stretching out in multiple dimensions was present (Fig. 3*D*), both intrafocal and extrafocal local networks shared a significantly reduced set of discernible states during the 40 s before LFP seizure onset [Fig. 3*A*, *B* (magnified portion), *E*]. Therefore, whereas intrafocal average population activity escalated toward electrographic seizure onset and extrafocal average population activity was much reduced, the transition toward electrographic seizures involved a reduced dimensionality in population activity in both compartments (Fig. 3*E*). Such a transition suggests a decline of the network into lower dimensional attractors (or semistable, theoretically recurrent population states) which has been proposed by computational simulations and EEG analysis (Mehta et al., 1993; Lopes da Silva

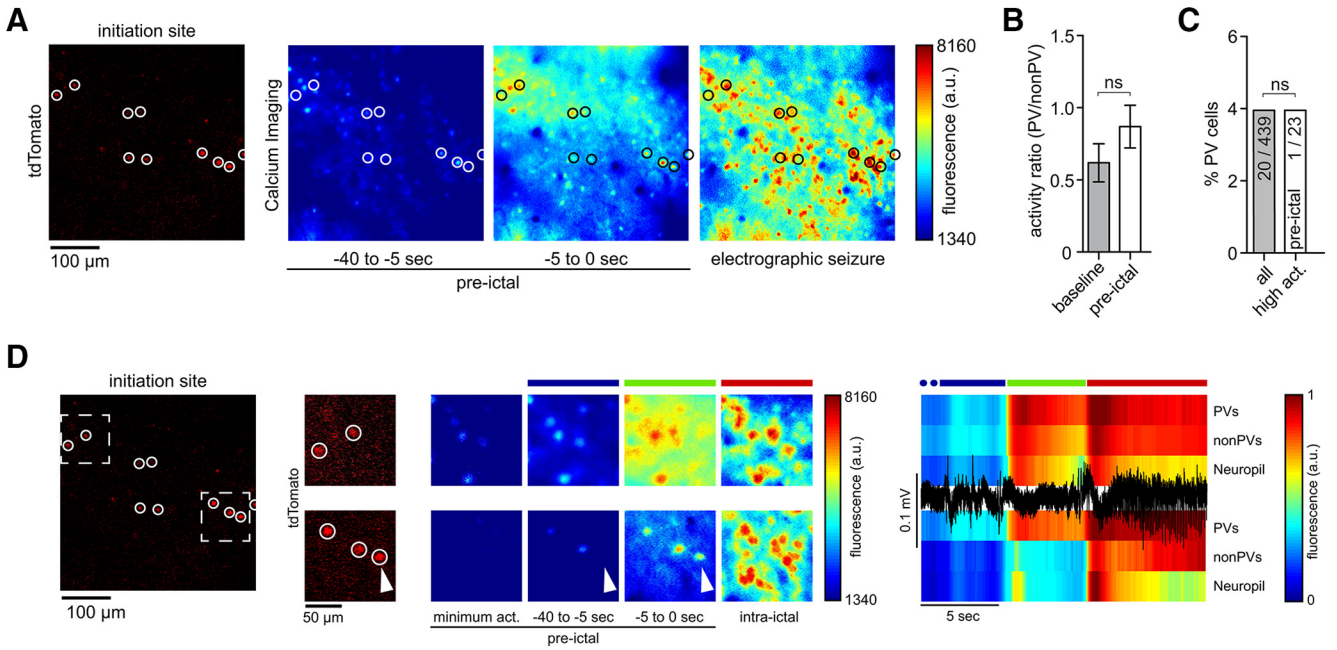

Figure 5. Ictal recruitment of PV interneurons in the seizure initiation site. ***A***, Left, tdTomato-positive parvalbumin containing interneurons (PVs, red, encircled) imaged at 990 nm; Ca^{2+} imaging (at 940 nm): fluorescence avg. images of pre-ictal and ictal neural activity. ***B***, Activity ratio of PV versus non-PV subpopulations during baseline and the 40 s period before LFP seizure onset. Activity ratios were obtained by dividing frame-subpopulation-averaged positive change of Ca^{2+} fluorescence ($n = 3$ exp., all imaged non-PVs = 439, all PVs = 20, 23 pre-ictal periods). During baseline (left), PVs continually displayed lower values than non-PVs. This relationship was preserved during the pre-ictal period (right, Mann–Whitney test $p = 0.4$). ns = not significant. ***C***, PV percentage among highest active neurons during pre-ictal period ($n = 3$ exp., 23 pre-ictal periods, top 5% activity cells = 23) compared with general subtype distribution (χ^2 test $P(\chi 2 > 0.002) = 1.0151$). ns = not significant. ***D***, Same exp. as in ***A*** with 2 magnified inserts (see also Movies 6 and 7) within distinct intrafocal subterritories. Ca^{2+} imaging during saltatory micro-epileptic progression (middle)**;** note again the diverse recruitment of PVs to ictal activity (arrowhead). Colored bars above the Ca^{2+} avg. images correspond to the colored bars above the LFP trace (black) and population avg. Ca^{2+} traces (PVs, non-PVs and Neuropil) on the right.

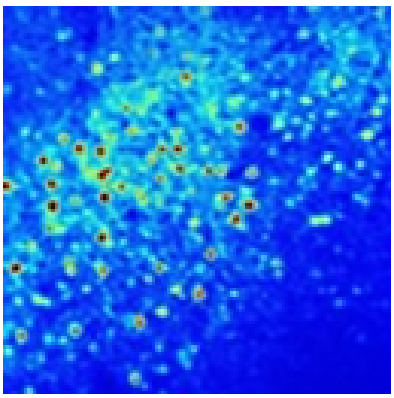

Movie 1. GCaMP6s calcium imaging of representative full ictal event within propagation area, left somatosensory cortex, layer II/III (depth ~150 μm beneath pial surface). The incoming wave corresponds to the electrographic seizure onset. Imaging wave length = 940 nm, acquisition speed = 30 frames/sec. Movie played at 2x acquisition speed.

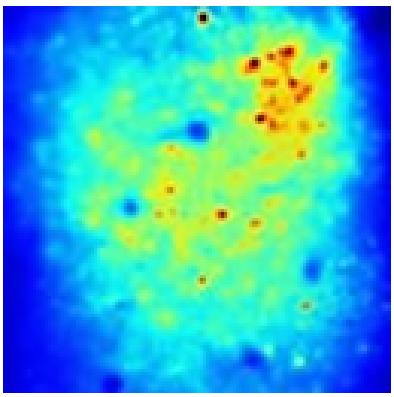

Movie 2. GCaMP6s calcium imaging of representative full ictal event within seizure initiation site, left somatosensory cortex, layer II/III (depth ~150 μm beneath pial surface). The final saltatory displayed step of microseizure expansion corresponds to the electrographic seizure onset. Note the striking difference in network recruitment duration, directionality, and continuity as compared to Movie 1. Imaging wave length = 940 nm, acquisition speed = 30 frames/sec. Movie played at 3x acquisition speed.

et al., 2003) to occur during ictal transition, but not directly documented at this spatiotemporal scale.

Together, we show that during epileptic expansion, intrafocal and extrafocal subnetworks of neurons activate differently. Although intrafocal population activity escalates toward LFP seizure onset, surround cortical subnetwork activity drops below baseline level. In both compartments, subnetwork activity declines into lower dimensional attractors during ictal transition.

Local PV interneuron populations enhance epileptic network compartmentalization

Recent *in vitro* and *in vivo* studies involving functional interference with interneuronal subtypes (especially fast-spiking PVs) have led to controversial results regarding the role of fast-spiking interneurons in seizure promotion or restraint (Avoli et al., 1993; Gnatkovsky et al., 2008; Avoli and de Curtis, 2011; Cammarota et al., 2013; Krook-Magnuson et al., 2013; Ledri et al., 2014; Shiri et al., 2015). With regard to interneuronal recruitment dynamics

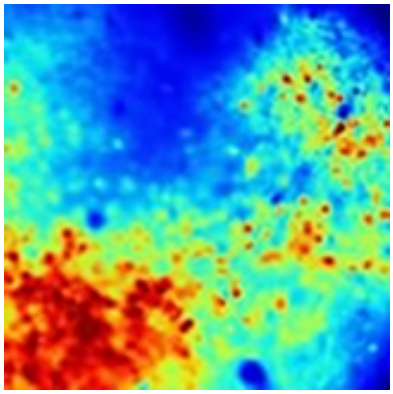

Movie 3. GCaMP6s calcium imaging of representative full ictal event within propagation area, left somatosensory cortex, layer II/III (depth ~150 μm beneath pial surface). The incoming wave corresponds to the electrographic seizure onset. Imaging wave length = 940 nm, acquisition speed = 30 frames/sec. Movie played at 3x acquisition speed.

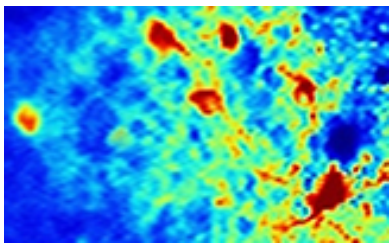

Movie 4. Magnified portion from Movie 3. GCaMP6s calcium imaging of representative full ictal event within propagation area, left somatosensory cortex, layer II/III (imaging depth ~150 μm beneath pial surface). Imaging wave length = 940 nm, acquisition speed = 30 frames/sec. Movie played at 4x acquisition speed.

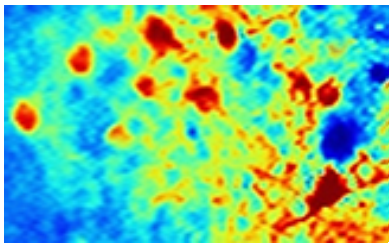

Movie 5. Magnified portion from Movie 3. GCaMP6s calcium imaging of representative successive full ictal event (in comparison to the earlier one displayed in Movie 4) within propagation area, left somatosensory cortex, layer II/III (imaging depth ~150 μm beneath pial surface). Imaging wave length = 940 nm, acquisition speed = 30 frames/sec. Movie played at 4x acquisition speed.

during epileptic activity, a recent study showed reliable recruitment of putative fast-spiking interneurons to epileptic activity (Neumann et al., 2017) echoing the finding of neural recruitment reliability at the general population level (Truccolo et al., 2011; Wenzel et al., 2017). Consistent with Muldoon et al. (2015), Neumann et al. (2017) also found that epileptic activity predominantly entrained PVs, not pyramidal cells. However, it remains unclear, whether these studies recorded inside the seizure initiation site, or surround cortex.

To understand the role of local GABAergic interneuron populations during seizure formation and spread, we studied calcium dynamics of PV interneurons in both intrafocal and extrafocal compartments by using transgenic mice that express the red fluorescent protein td-Tomato in parvalbumin containing interneurons (Madisen et al., 2010). First, we simultaneously imaged PV and non-PV calcium dynamics during seizure spread into the propagation area (extrafocal, Fig. 4*A*, Movie 3). Interestingly, PVs were consistently among the neurons displaying the strongest calcium activity during the 40 s time period leading up to an electrographic seizure (Fig. 4*B*). Population-level analyses further supported this finding. Although absolute activity (e.g., firing rates) could not be directly compared between PV cells and non-PV cells given known differences in cell calcium dynamics, bursting patterns, and baseline rates (Hofer et al., 2011), the relative ratio of PV versus non-PV population calcium transients was inverted during the 40 s period before electrographic seizures compared with baseline conditions (Fig. 4*C*), suggesting that PVs comprise a functionally distinct subpopulation in the propagation area during seizure formation (Neumann et al., 2017; Liou et al., 2018). During epileptic invasion of extrafocal territories during electrographic seizures, we encountered surprisingly eclectic PV population dynamics with several striking features. In accordance with previous reports, we identified PVs that reliably showed strong calcium transients just ahead of the arriving seizure wavefront (Fig. 4*D*, cells 1 and 3) (Kawaguchi, 2001; Timofeev et al., 2002; Trevelyan et al., 2006; Ziburkus et al., 2006; Schevon et al., 2012; Cammarota et al., 2013). At the same time however, we found at times immediately neighboring PVs displaying delayed recruitment (Cell 2 and 5 in Fig. 4 *D*,*E*). Consistent with the electrophysiological data by Neumann and colleagues (Neumann et al., 2017), these sequential PV calcium dynamics were conserved across seizures (Fig. 4*E*). Surprisingly, we also identified transiently nonparticipant PVs (cell 4 in Fig. 4*D*, top; Fig. 4*E*, Movie 4). Clear recruitment to later seizures (cell 4 in Fig. 4*D*, bottom; Fig. 4*E*, Movie 5) excluded the possibility of a lack of GCaMP expression.

Finally, we went on to image subpopulation dynamics within the seizure initiation site (Fig. 5*A*). Consistent with our results in extrafocal territories, PVs showed less population average calcium activity than non-PVs at baseline (Fig. 5*B*, left). By contrast, after 4-AP injection, this relationship was not inverted in the 40 s before electrographic seizure onset (Fig. 5*B*, right). We also did not encounter an increased percentage of intrafocal PVs among the neurons displaying highest calcium activity during the final 40 s before electrographic seizure onset. This does not indicate that intrafocal PVs were less active but rather that they were surrounded by enhanced local firing of non-PV cells (Fig. 5*C*). Interestingly, similar to our results in extrafocal territories, in small intrafocal patches of cortex during epileptic expansion before LFP seizure onset, we found diverse local recruitment of PVs as well (Fig. 5*D*, arrowheads). During intrafocal epileptic microprogression, we observed stepwise failure of the inhibitory surround (Trevelyan et al., 2006; Cammarota et al., 2013) (Fig. 5 *A*, *D*; Fig. 5*D*, blue bars, Movies 6 and 7).

We conclude that PVs display spatially heterogeneous recruitment patterns within epileptic networks. Before electrographic seizure onset, a hypoactive surround cortex, and even small hypoactive regions ($<100\ \mu m^2$) within the seizure initiation site, are observed together with increased local PV population activity. On an average population level, PVs increase their firing during ictal transition, consistent with previous studies (Prince and Wilder, 1967; Schwartz and Bonhoeffer, 2001; Timofeev et al., 2002; Gnatkovsky et al., 2008; Cammarota et al., 2013; Miri et al.,

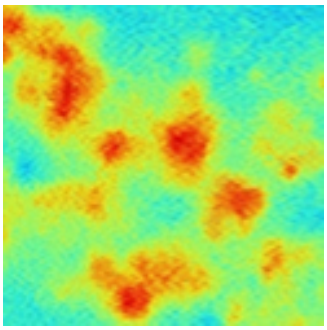

Movie 6. Magnified portion imaged field of view as displayed in Figure 5 *A* and *D* (upper left). GCaMP6s calcium imaging of step-wise microepileptic expansion within the seizure initiation site, left somatosensory cortex, layer II/III (imaging depth ~150 μm beneath pial surface). Imaging wave length = 940 nm, acquisition speed = 30 frames/sec. Movie is played 4x acquisition speed.

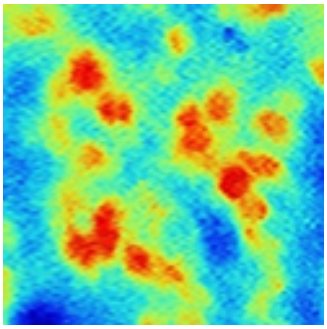

Movie 7. Magnified portion imaged field of view as displayed in Figure 5 *A* and *D* (lower right). GCaMP6s calcium imaging of step-wise microepileptic expansion within the seizure initiation site, left somatosensory cortex, layer II/III (imaging depth ~150 μm beneath pial surface). Imaging wave length = 940 nm, acquisition speed = 30 frames/second. Movie is played at 4x acquisition speed.

2018). However, at the single-cell level, we find side-by-side early and late PV recruitment in a spatially heterogeneous fashion, and even nonparticipant PVs. The temporal patterns of sequential PV activation repeat across seizures (Neumann et al., 2017).

Discussion

To better understand how seizures originate, we used an *in vivo* mouse model of acute pharmacological seizures induced by local cortical 4-AP injection (Zhao et al., 2011; Ma et al., 2013; Wenzel et al., 2017; Liou et al., 2018), a widely established model of focal onset seizures that enables the establishment of a precisely defined seizure initiation site. We used calcium imaging to study cortical circuit activity within the seizure initiation site, and in primarily unperturbed surround cortex at a distance of 1.5–2 mm during secondary seizure spread (Nagappan et al., 2018, please also see methods).

We find aberrant intrafocal activity that occurs before LFP seizure detection, which in our view corresponds to seizure initiation at the anatomical microscale (Goldensohn, 1975; Schevon et al., 2008; Worrell et al., 2008; Stead et al., 2010). Studies using multielectrode arrays (MEA) have suggested that sustained micro-epileptic activity represents the earliest step during seizure emergence (Goldensohn, 1975; Bragin et al., 2000; Schevon et al., 2008; Worrell et al., 2008; Stead et al., 2010). However, this has been difficult to definitely prove using MEAs in humans, as the most common arrays cover a cortical area of 4 × 4 mm and contain 96 electrodes spaced 400 μm apart. As a consequence, full temporal seizure evolution will likely be missed, since the seizure initiation site can be as small as 0.04 mm^3 (Schevon et al., 2008). Our intrafocal imaging with single-cell resolution supports the hypothesis that the hyperactivity of pathologically interconnected neuronal clusters (PINs) serve as a prerequisite of seizures that are then detected by field electrophysiology (Bragin et al., 2000). This spatially confined, evolving intrafocal population activity preceding the electrographic seizure onset may be described as ictal activity that is 'electrographically silent', like an electrographic seizure in the surface EEG that occurs in the absence of clinical symptoms is typically called 'clinically silent' in medical practice. Naturally, there can be no epileptic activity of any sort that is electrically silent, as it is inherently based on neural activity. However, this does not preclude the notion that an electrical signal can be electrographically 'silent' depending on the resolution of the recording technique (e.g., a single neuron's activity cannot be detected by an EEG macroelectrode). However, as our intrafocal experiments did not include simultaneous optical and electrical recordings at the exact same location, our data does not unambiguously prove that neuronal ensemble activation before electrographic seizure onset (detected by the nearby microelectrode) corresponds to initial microseizure activity. Thus, it is also possible that the calcium data corresponded to pre-ictal population bursts recruiting increasingly large ensembles over time (Huberfeld et al., 2011). However, consistent with a recent case report of a microseizure (LFP) preceding macroseizure onset (intracranial EEG, or iEEG) in a patient (Weiss et al., 2016), it remains plausible that our intrafocal imaging indeed captured seizure initiation, as the escalating intrafocal population activity consistently transitioned over into the electrographic seizure, was sustained, aberrant, and evolved in time and space. The latter activity features are essential parameters in identifiying seizure activity in EEG recordings in clinical routine.

To our knowledge, no *in vivo* study to date has captured the very first step of a seizure on the scale of local microcircuits. In fact, due to the potentially miniscule neural starter population and the rapid decay of LFP signal strength with distance, it was recently hypothesized that it might be impossible to precisely capture seizure initiation in humans using field electrophysiology (Schevon et al., 2019).

Our approach, using fast two-photon calcium imaging *in vivo*, enabled us to follow acute seizure evolution from its earliest time point in the intact brain. We observed differential modes of spatiotemporal microprogression of epileptic activity inside the seizure initiation site compared with epileptic invasion of the propagation area. Inside the initiation site, we found a saltatory (i.e., "stepwise," "modular," or "discontinuous") expansion of epileptic activity on the time scale of seconds (Trevelyan et al., 2006). Consistent with studies on extrafocal seizure propagation in animals (Schwartz and Bonhoeffer, 2001; Ma et al., 2013) and humans (Schevon et al., 2012), intrafocal expansion of aberrant activity was followed by a more continuous seizure spread into nearby cortex during electrographic seizures, which suggests that seizure evolution consists of different consecutive types of progression across anatomical scales (Fig. 6, schematic overview).

Even though pathological local networks (Mehta et al., 1993; Bower et al., 2015) and local interaction of excitatory and inhibitory neurons within epileptic networks (Bragin et al., 2000) have been suggested to play a pivotal role in the progression of ictal activity (for review, see Trevelyan and Schevon, 2013), little is known about their fine-scale *in vivo* subpopulation dynamics

within cortical microcircuits. Our data indicate that interneuron activity compartmentalizes local cortical networks before electrographic seizures, and throughout seizure evolution, with distinct local footprints of neural subpopulation dynamics. In the 40 s leading up to the electrographic seizure, intrafocal population average dynamics comprised pathologically high and escalating pyramidal cell firing in the presence of enhanced interneuron population average activity while at the same time yet-to-be-invaded ("penumbral") extrafocal territories displayed enhanced interneuron firing and suppressed pyramidal activity. At an even finer anatomical scale (dozens of micrometers), the described local subpopulation footprints of activity could be observed also within the seizure initiation site. In studies on ictal neural recruitment in the context of chronic epilepsy, the precise spatial origin of a recorded seizure cannot be experimentally controlled. As a consequence, the exact location of recording with regards to the seizure initiation site at the anatomical microscale remains usually vague. Our subpopulation imaging results could facilitate the retroactive determination of the recording location (e.g., intrafocal vs extrafocal) in studies investigating seizures in humans or animal models of chronic epilepsy, even in the absence of a priori knowledge about where exactly a seizure started. For example, in a recent study investigating LVF seizures using microwires and macroelectrodes in patients with temporal lobe epilepsy, it was reported that putative interneurons in the mesial temporal lobe increase their firing seconds ahead of putative excitatory neurons within both the macroanatomically defined SOZ (ipsilateral) and propagation areas (contralateral) (Elahian et al., 2018). Based on the microanatomical data presented here, and a previous report of a single LVF seizure in a human (Weiss et al., 2016), where the macroelectrographic (intracranial EEG) seizure onset was preceded by an LFP microseizure, it could be reasonably assumed that the areas sampled by Elahian et al. (2018) within the macroanatomical SOZ were exclusively located outside the microanatomical seizure initiation site, and invaded only during seizure spread (which was discussed by the authors themselves).

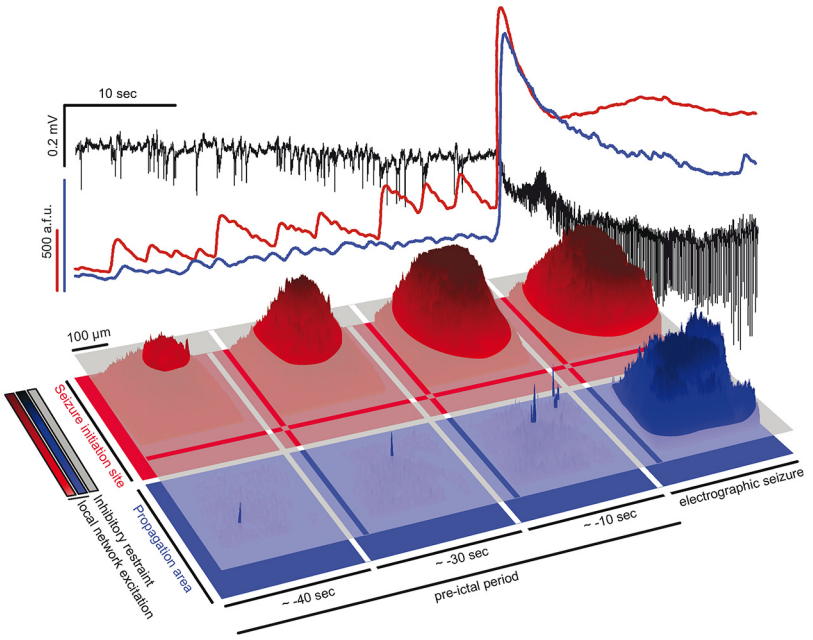

Figure 6. Two-step seizure progression model. Top panel: Depicted is a 40 s pre-ictal period before electrographic seizure onset, and initial 20 s of a full ictal event. LFP (black), and corresponding intrafocal (red) and extrafocal (blue) avg. population Ca^{2+} transient. Note how during the pre-ictal period, increasingly escalating population Ca^{2+} events are only detected inside the seizure initiation site, not in extrafocal territories. Bottom, Corresponding to the population avg. signals shown above, 3-D surface Ca^{2+} activity plots of imaged fields of view inside the seizure initiation site (red), and in extrafocal territory (blue). The gray layer schematically represents local interneuron population activity. During intrafocal micro-epileptic build-up in the pre-ictal period, inhibition fails at the level of local ensembles only inside the seizure initiation site. Small patches of excitatory ensemble activity break through the layer of local inhibition. Microepileptic expansion over the 40 s pre-ictal period occurs in a saltatory fashion taking over increasingly large areas where inhibition has failed to restrain epileptic activity. Due to the yet highly spatially confined epileptic build-up, it is at first electrographically silent, and not detected even by nearby LFP microelectrodes. Once a local threshold is reached (whose nature remains unclear), seizures spread into neighboring territories outside the seizure initiation site in a continuous fashion, and become detectable by microelectrodes and macroelectrodes across wider portions of the brain. Before this ictal expansion, little population activity can be detected in surround cortex, as opposed to intrafocal territories. This is likely due to increased feedforward inhibition in extrafocal areas that is driven by locally confined pathological activity inside the seizure initiation site. Thus, seizure progression consists of at least two consecutive steps, and may display differential spatiotemporal local network and subpopulation dynamics highly depending on the localization of recording.

Does interneuron activity restrain, or promote seizures? Consistent with previous work *in vivo*, we found enhanced local interneuron activity immediately before electrographic seizures (Prince and Wilder, 1967; Miri et al., 2018). Although some studies suggest that it is this enhanced pre-ictal interneuronal firing that triggers seizures by pathological entrainment of excitatory neurons (Shiri et al., 2015; Avoli et al., 2016; Miri et al., 2018), there is also *in vitro* (Ziburkus et al., 2006; Sessolo et al., 2015) and *in vivo* (Jayant et al., 2019) evidence based on intracellular recordings that local progression of epileptic activity coincides with interneuronal depolarization block. Our data rather support the latter studies in that we find enhanced pre-ictal interneuronal activity while at the same time immediate surround pyramidal cell firing is not increasingly synchronized, but in fact suppressed. Still, sustained interneuronal activity may support network synchronization by rebound excitation upon inhibitory failure (Grenier et al., 1998; Sessolo et al., 2015). Along these lines, it is possible that the LFP paroxysmal depolarization shift observed during electrographical seizures in our experiments, corresponds to tonic firing of excitatory neurons upon inhibitory failure at the anatomical macroscale (Baldino et al., 1986; Traub et al., 1993; Stiglbauer et al., 2017). It is of important note that seizure promoting, restraining, or sustaining effects of interneuronal activity likely highly depend on the microanatomical location (e.g., seizure initiation site vs propagation area) (Sessolo et al., 2015; Khoshkhoo et al., 2017; Codadu et al., 2019), timing and regularity of interneuronal activity (Uva et al., 2013; Khoshkhoo et al., 2017; Shiri et al., 2017; Miri et al., 2018), and interneuronal subtype (Khoshkhoo et al., 2017). Further, findings on seizure promoting or restraining interneuron dynamics may be restricted to the used experimental model (i.e., local 4-AP model). Notably, it never occurred in our experiments that all PVs in the field of view ($\sim$400 $\times$ 400 μm) showed simultaneous preseizure calcium transients indicating that the elicitation of epileptic discharges by simultaneous optogenetic activation of large PV populations might not reflect the *in vivo* situation (Shiri et al., 2015).

Echoing our and other research groups' recent analyses of local ictal network recruitment in time (Truccolo et al., 2014; Rossi et al., 2017; Wenzel et al., 2017), we found that temporal activation of local PVs is conserved across seizures (Neumann et al., 2017). Although seemingly at odds with previous reports on temporal heterogeneity of neural recruitment to seizures (Bower et al., 2012), we find it important to note that this discrepancy might be based on a missing distinction between absolute and relative time scales. Although our data indicate substantial reliability (or "stereotypy" or "homogeneity") of neural recruitment on relative time scales, that is, order of recruitment, we found, at the same time, profound recruitment heterogeneity (or "variability" or "elasticity") on absolute time scales (Wenzel et al., 2017).

A main finding of the present study is that spatial recruitment of local PVs during seizures is highly diverse, extending from previous studies showing that interneurons fire ahead of the propagating seizure wave front (Kawaguchi, 2001; Timofeev et al., 2002; Trevelyan et al., 2006; Ziburkus et al., 2006; Schevon et al., 2012; Cammarota et al., 2013). At times, immediately neighboring PVs (intercell distance <20 μm) showed completely different temporal activation during seizure break-in indicating that the PV subfamily does not activate homogeneously during seizures. It seems intuitive that one main reason for this should be rooted in within-class molecular PV subtypes (e.g., chandelier cells vs basket cells), and their differential connectivity. However, due to a lack of spatial resolution in most studies, and current constraints in molecular targeting of within-class interneuron subtypes, this diversity of spatial recruitment of local PVs to seizures has been largely overlooked. Intriguingly, because of double fluorescent labeling and the high spatial resolution of our imaging approach, we also found nonparticipant PVs during seizures. Since PVs can synapse onto each other and are also targets of other interneuronal classes (Sik et al., 1995; Bezaire and Soltesz, 2013; Pfeffer et al., 2013; Pi et al., 2013), nonparticipant PVs, and potentially other inhibitory subtypes as well, may be actively inhibited during seizures (Paz and Huguenard, 2015). This finding might help understand why *in vivo* optogenetic activation of PVs during seizures still suspended epileptic activity (Krook-Magnuson et al., 2013), in a circumstance where one would assume PVs to be strongly active anyway. In those experiments, light activation might have recruited predominantly "nonexhausted" PVs.

In summary, we provide novel insights into the microcircuit dynamics across seizure evolution from its earliest time point *in vivo*, demonstrating how local synchronization of neuronal ensembles evolves into electrographically detectable seizures. Our experiments help viewing differential modes of seizure microprogression within a larger context of seizure evolution, and show that PV population dynamics during seizures in extrafocal and intrafocal regions are spatially more diverse than previously thought. Our results also underscore that the precise location of recording is critical to any one experiment investigating seizure microprogression. Here, we establish spatiotemporal subtype activity footprints that correspond to consecutive steps of seizure microprogression. As in chronic focal epilepsy the precise seizure initiation site is often unclear, such footprints could instruct high-resolution recordings in determining the recording location (e.g., intrafocal vs extrafocal) even in the absence of *a priori* knowledge about where exactly a seizure started.

References

Arida RM, Scorza FA, Peres CA, Cavalheiro EA (1999) The course of untreated seizures in the pilocarpine model of epilepsy. Epilepsy Res 34:99–107.

Avoli M, de Curtis M (2011) GABAergic synchronization in the limbic system and its role in the generation of epileptiform activity. Prog Neurobiol 95:104–132.

Avoli M, Psarropoulou C, Tancredi V, Fueta Y (1993) On the synchronous activity induced by 4-aminopyridine in the CA3 subfield of juvenile rat hippocampus. J Neurophysiol 70:1018–1029.

Avoli M, D'Antuono M, Louvel J, Köhling R, Biagini G, Pumain R, D'Arcangelo G, Tancredi V (2002) Network and pharmacological mechanisms leading to epileptiform synchronization in the limbic system in vitro. Prog Neurobiol 68:167–207.

Avoli M, de Curtis M, Gnatkovsky V, Gotman J, Kohling R, Lévesque M, Manseau F, Shiri Z, Williams S (2016) Specific imbalance of excitatory/inhibitory signaling establishes seizure onset pattern in temporal lobe epilepsy. J Neurophysiol 115:3229–3237.

Badea T, Goldberg J, Mao B, Yuste, R (2001) Calcium imaging of epileptiform events with single-cell resolution. J Neurobiol 215–227.

Baldino F Jr, Wolfson B, Heinemann U, Gutnick MJ (1986) An N-methyl-D-aspartate (NMDA) receptor antagonist reduces bicuculline-induced depolarization shifts in neocortical explant cultures. Neurosci Lett 70:101–105.

Beleza P (2012) Acute symptomatic seizures: a clinically oriented review. Neurologist 18:109–119.

Bezaire MJ, Soltesz I (2013) Quantitative assessment of CA1 local circuits: knowledge base for interneuron-pyramidal cell connectivity. Hippocampus 23:751–785.

Bower MR, Buckmaster PS (2008) Changes in granule cell firing rates precede locally recorded spontaneous seizures by minutes in an animal model of temporal lobe epilepsy. J Neurophysiol 99:2431–2442.

Bower MR, Stead M, Meyer FB, Marsh WR, Worrell GA (2012) Spatiotemporal neuronal correlates of seizure generation in focal epilepsy. Epilepsia 53:807–816.

Bower MR, Stead M, Bower RS, Kucewicz MT, Sulc V, Cimbalnik J, Brinkmann BH, Vasoli VM, St Louis EK, Meyer FB, Marsh WR, Worrell GA (2015) Evidence for consolidation of neuronal assemblies after seizures in humans. J Neurosci 35:999–1010.

Bragin A, Wilson CL, Engel J Jr (2000) Chronic epileptogenesis requires development of a network of pathologically interconnected neuron clusters: a hypothesis. Epilepsia 41:S144–S152.

Cammarota M, Losi G, Chiavegato A, Zonta M, Carmignoto G (2013) Fast spiking interneuron control of seizure propagation in a cortical slice model of focal epilepsy. J Physiol 591:807–822.

Cattell RB (1966) The scree test for the number of factors. Multivariate Behavioral Research 1:245–276.

Chen TW, Wardill TJ, Sun Y, Pulver SR, Renninger SL, Baohan A, Schreiter ER, Kerr RA, Orger MB, Jayaraman V, Looger LL, Svoboda K, Kim DS (2013) Ultrasensitive fluorescent proteins for imaging neuronal activity. Nature 499:295–300.

Codadu NK, Parrish RR, Trevelyan AJ (2019) Region-specific differences and areal interactions underlying transitions in epileptiform activity. J Physiol 597:2079–2096.

Elahian B, Lado NE, Mankin E, Vangala S, Misra A, Moxon K, Fried I, Sharan A, Yeasin M, Staba R, Bragin A, Avoli M, Sperling MR, Engel J Jr, Weiss SA (2018) Low-voltage fast seizures in humans begin with increased interneuron firing. Ann Neurol 84:588–600.

Ewell LA, Liang L, Armstrong C, Soltész I, Leutgeb S, Leutgeb JK (2015) Brain state is a major factor in preseizure hippocampal network activity and influences success of seizure intervention. J Neurosci 35:15635–15648.

Feldt Muldoon S, Soltesz I, Cossart R (2013) Spatially clustered neuronal assemblies comprise the microstructure of synchrony in chronically epileptic networks. Proc Natl Acad Sci U S A 110:3567–3572.

Gnatkovsky V, Librizzi L, Trombin F, de Curtis M (2008) Fast activity at seizure onset is mediated by inhibitory circuits in the entorhinal cortex in vitro. Ann Neurol 64:674–686.

Goldensohn ES (1975) Initiation and propagation of epileptogenic foci. Adv Neurol 11:141–162.

Grenier F, Timofeev I, Steriade M (1998) Leading role of thalamic over

cortical neurons during postinhibitory rebound excitation. Proc Natl Acad Sci U S A 95:13929–13934.
Hofer SB, Ko H, Pichler B, Vogelstein J, Ros H, Zeng H, Lein E, Lesica NA, Mrsic-Flogel TD (2011) Differential connectivity and response dynamics of excitatory and inhibitory neurons in visual cortex. Nat Neurosci 14:1045–1052.
Howe J, Lu X, Thompson Z, Peterson GW, Losey TE (2016) Intraoperative seizures during craniotomy under general anesthesia. Seizure 38:23–25.
Huberfeld G, Menendez de la Prida L, Pallud J, Cohen I, Le Van Quyen M, Adam C, Clemenceau S, Baulac M, Miles R (2011) Glutamatergic pre-ictal discharges emerge at the transition to seizure in human epilepsy. Nat Neurosci 14:627–634.
Jayant K, Wenzel M, Bando Y, Hamm JP, Mandriota N, Rabinowitz JH, Plante IJ, Owen JS, Sahin O, Shepard KL, et al. (2019) Flexible nanopipettes for minimally invasive intracellular electrophysiology in vivo. Cell Rep *26* 266–278 e265.
Jirsa VK, Stacey WC, Quilichini PP, Ivanov AI, Bernard C (2014) On the nature of seizure dynamics. Brain 137:2210–2230.
Kaiser HF (1958) The varimax criterion for analytic rotation in factor analysis. Psychometrika 23:187–200.
Kawaguchi Y (2001) Distinct firing patterns of neuronal subtypes in cortical synchronized activities. J Neurosci 21:7261–7272.
Khoshkhoo S, Vogt D, Sohal VS (2017) Dynamic, cell-type-specific roles for GABAergic interneurons in a mouse model of optogenetically inducible seizures. Neuron 93:291–298.
Krook-Magnuson E, Armstrong C, Oijala M, Soltesz I (2013) On-demand optogenetic control of spontaneous seizures in temporal lobe epilepsy. Nat Commun 4:1376.
Ledri M, Madsen MG, Nikitidou L, Kirik D, Kokaia M (2014) Global optogenetic activation of inhibitory interneurons during epileptiform activity. J Neurosci 34:3364–3377.
Lillis KP, Wang Z, Mail M, Zhao GQ, Berdichevsky Y, Bacskai B, Staley KJ (2015) Evolution of network synchronization during early epileptogenesis parallels synaptic circuit alterations. J Neurosci 35:9920–9934.
Liou JY, Ma H, Wenzel M, Zhao M, Baird-Daniel E, Smith EH, Daniel A, Emerson R, Yuste R, Schwartz TH, Schevon CA (2018) Role of inhibitory control in modulating spread of focal ictal activity. Brain 141: 2083–2097
Lopes da Silva F, Blanes W, Kalitzin SN, Parra J, Suffczynski P, Velis DN (2003) Epilepsies as dynamical diseases of brain systems: basic models of the transition between normal and epileptic activity. Epilepsia 44:72–83.
Ma H, Zhao M, Schwartz TH (2013) Dynamic neurovascular coupling and uncoupling during ictal onset, propagation, and termination revealed by simultaneous in vivo optical imaging of neural activity and local blood volume. Cereb Cortex 23:885–899.
Madisen L, Zwingman TA, Sunkin SM, Oh SW, Zariwala HA, Gu H, Ng LL, Palmiter RD, Hawrylycz MJ, Jones AR, Lein ES, Zeng H (2010) A robust and high-throughput cre reporting and characterization system for the whole mouse brain. Nat Neurosci 13:133–140.
Mehta MR, Dasgupta C, Ullal GR (1993) A neural network model for kindling of focal epilepsy: basic mechanism. Biol Cybern 68:335–340.
Miller JE, Ayzenshtat I, Carrillo-Reid L, Yuste R (2014) Visual stimuli recruit intrinsically generated cortical ensembles. Proc Natl Acad Sci U S A 111:E4053–4061.
Milton JG, Chkhenkeli SA, Towle VL (2007) Brain connectivity and the spread of epileptic seizures. In: Handbook of brain connectivity, pp 477–503. Heidelberg: Springer.
Miri ML, Vinck M, Pant R, Cardin JA (2018) Altered hippocampal interneuron activity precedes ictal onset. Elife 7:e40750.
Muldoon SF, Villette V, Tressard T, Malvache A, Reichinnek S, Bartolomei F, Cossart R (2015) GABAergic inhibition shapes interictal dynamics in awake epileptic mice. Brain 138:2875–2890.
Nagappan S, Liu L, Fetcho R, Nguyen J, Nishimura N, Radwanski RE, Lieberman S, Baird-Daniel E, Ma H, Zhao M, Schaffer CB, Schwartz TH (2018) In vivo femtosecond laser subsurface cortical microtransections attenuate acute rat focal seizures. Cereb Cortex. In press.
Neubauer FB, Sederberg A, MacLean JN (2014) Local changes in neocortical circuit dynamics coincide with the spread of seizures to thalamus in a model of epilepsy. Front Neural Circuits 8:101.
Neumann AR, Raedt R, Steenland HW, Sprengers M, Bzymek K, Navratilova Z, Mesina L, Xie J, Lapointe V, Kloosterman F, Vonck K, Boon PAJM, Soltesz I, McNaughton BL, Luczak A (2017) Involvement of fast-spiking cells in ictal sequences during spontaneous seizures in rats with chronic temporal lobe epilepsy. Brain 140:2355–2369.
Paz JT, Huguenard JR (2015) Microcircuits and their interactions in epilepsy: is the focus out of focus? Nat Neurosci 18:351–359.
Pfeffer CK, Xue M, He M, Huang ZJ, Scanziani M (2013) Inhibition of inhibition in visual cortex: the logic of connections between molecularly distinct interneurons. Nat Neurosci 16:1068–1076.
Pi HJ, Hangya B, Kvitsiani D, Sanders JI, Huang ZJ, Kepecs A (2013) Cortical interneurons that specialize in disinhibitory control. Nature 503:521–524.
Prince DA, Wilder BJ (1967) Control mechanisms in cortical epileptogenic foci. "Surround" inhibition. Arch Neurol 16:194–202.
Rossi LF, Wykes RC, Kullmann DM, Carandini M (2017) Focal cortical seizures start as standing waves and propagate respecting homotopic connectivity. Nat Commun 8:217.
Schevon CA, Ng SK, Cappell J, Goodman RR, McKhann G Jr, Waziri A, Branner A, Sosunov A, Schroeder CE, Emerson RG (2008) Microphysiology of epileptiform activity in human neocortex. J Clin Neurophysiol 25:321–330.
Schevon CA, Weiss SA, McKhann G Jr, Goodman RR, Yuste R, Emerson RG, Trevelyan AJ (2012) Evidence of an inhibitory restraint of seizure activity in humans. Nat Commun 3:1060.
Schevon CA, Tobochnik S, Eissa T, Merricks E, Gill B, Parrish RR, Bateman LM, McKhann GM Jr, Emerson RG, Trevelyan AJ (2019) Multiscale recordings reveal the dynamic spatial structure of human seizures. Neurobiol Dis 127:303–311.
Schwartz TH, Bonhoeffer T (2001) In vivo optical mapping of epileptic foci and surround inhibition in ferret cerebral cortex. Nat Med 7:1063–1067.
Sessolo M, Marcon I, Bovetti S, Losi G, Cammarota M, Ratto GM, Fellin T, Carmignoto G (2015) Parvalbumin-positive inhibitory interneurons oppose propagation but favor generation of focal epileptiform activity. J Neurosci 35:9544–9557.
Shiri Z, Manseau F, Lévesque M, Williams S, Avoli M (2015) Interneuron activity leads to initiation of low-voltage fast-onset seizures. Ann Neurol 77:541–546.
Shiri Z, Lévesque M, Etter G, Manseau F, Williams S, Avoli M (2017) Optogenetic low-frequency stimulation of specific neuronal populations abates ictogenesis. J Neurosci 37:2999–3008.
Sik A, Penttonen M, Ylinen A, Buzsáki G (1995) Hippocampal CA1 interneurons: an in vivo intracellular labeling study. J Neurosci 15:6651–6665.
Smetters D, Majewska A, Yuste R (1999) Detecting action potentials in neuronal populations with calcium imaging. Methods 18:215–221.
Stead M, Bower M, Brinkmann BH, Lee K, Marsh WR, Meyer FB, Litt B, Van Gompel J, Worrell GA (2010) Microseizures and the spatiotemporal scales of human partial epilepsy. Brain 133:2789–2797.
Stiglbauer V, Hotka M, Ruiß M, Hilber K, Boehm S, Kubista H (2017) Cav 1.3 channels play a crucial role in the formation of paroxysmal depolarization shifts in cultured hippocampal neurons. Epilepsia 58:858–871.
Szente M, Pongrácz F (1979) Aminopyridine-induced seizure activity. Electroencephalogr Clin Neurophysiol 46:605–608.
Tashiro A, Goldberg J, Yuste R (2002) Calcium oscillations in neocortical astrocytes under epileptiform conditions. J Neurobiol 50:45–55.
Timofeev I, Grenier F, Steriade M (2002) The role of chloride-dependent inhibition and the activity of fast-spiking neurons during cortical spike-wave electrographic seizures. Neuroscience 114:1115–1132.
Traub RD, Miles R, Jefferys JG (1993) Synaptic and intrinsic conductances shape picrotoxin-induced synchronized after-discharges in the guinea-pig hippocampal slice. J Physiol 461:525–547.
Trevelyan AJ, Schevon CA (2013) How inhibition influences seizure propagation. Neuropharmacology 69:45–54.
Trevelyan AJ, Sussillo D, Watson BO, Yuste R (2006) Modular propagation of epileptiform activity: evidence for an inhibitory veto in neocortex. J Neurosci 26:12447–12455.
Trevelyan AJ, Sussillo D, Yuste R (2007) Feedforward inhibition contributes to the control of epileptiform propagation speed. J Neurosci 27:3383–3387.
Truccolo W, Donoghue JA, Hochberg LR, Eskandar EN, Madsen JR, Anderson WS, Brown EN, Halgren E, Cash SS (2011) Single-neuron dynamics in human focal epilepsy. Nat Neurosci 14:635–641.

Truccolo W, Ahmed OJ, Harrison MT, Eskandar EN, Cosgrove GR, Madsen JR, Blum AS, Potter NS, Hochberg LR, Cash SS (2014) Neuronal ensemble synchrony during human focal seizures. J Neurosci 34:9927–9944.

Ulkatan S, Jaramillo AM, Téllez MJ, Kim J, Deletis V, Seidel K (2017) Incidence of intraoperative seizures during motor evoked potential monitoring in a large cohort of patients undergoing different surgical procedures. J Neurosurg 126:1296–1302.

Uva L, Trombin F, Carriero G, Avoli M, de Curtis M (2013) Seizure-like discharges induced by 4-aminopyridine in the olfactory system of the in vitro isolated guinea pig brain. Epilepsia 54:605–615.

Warren CP, Hu S, Stead M, Brinkmann BH, Bower MR, Worrell GA (2010) Synchrony in normal and focal epileptic brain: the seizure onset zone is functionally disconnected. J Neurophysiol 104:3530–3539.

Weiss SA, Alvarado-Rojas C, Bragin A, Behnke E, Fields T, Fried I, Engel J Jr, Staba R (2016) Ictal onset patterns of local field potentials, high frequency oscillations, and unit activity in human mesial temporal lobe epilepsy. Epilepsia 57:111–121.

Wenzel M, Hamm JP, Peterka DS, Yuste R (2017) Reliable and elastic propagation of cortical seizures in vivo. Cell Rep 19:2681–2693.

Wong BY, Prince DA (1990) The lateral spread of ictal discharges in neocortical brain slices. Epilepsy Res 7:29–39.

Worrell GA, Gardner AB, Stead SM, Hu S, Goerss S, Cascino GJ, Meyer FB, Marsh R, Litt B (2008) High-frequency oscillations in human temporal lobe: simultaneous microwire and clinical macroelectrode recordings. Brain 131:928–937.

Yuste R, Katz LC (1991) Control of postsynaptic Ca2+ influx in developing neocortex by excitatory and inhibitory neurotransmitters. Neuron 6:333–344.

Zhao M, Nguyen J, Ma H, Nishimura N, Schaffer CB, Schwartz TH (2011) Pre-ictal and ictal neurovascular and metabolic coupling surrounding a seizure focus. J Neurosci 31:13292–13300.

Ziburkus J, Cressman JR, Barreto E, Schiff SJ (2006) Interneuron and pyramidal cell interplay during in vitro seizure-like events. J Neurophysiol 95:3948–3954.